MOISTURE AND SOLUTE FLUX ALONG PREFERRED PATHWAYS CHARACTERIZED BY FISSURED SEDIMENTS IN DESERT SOILS*

Bridget R. Scanlon

Bureau of Economic Geology, The University of Texas at Austin, Austin, TX 78713-7508, U.S.A
(Recieved June 1990; revised and accepted 23 January 1991)

ABSTRACT

Evaluation of preferred flow pathways is critical for waste disposal. These pathways reduce the effectiveness of thick desert soils in attenuating contaminants by short-circuiting flow through the unsaturated zone. Unsaturated flow in fissured sediments in the Chihuahuan Desert of Texas was examined to determine if these sediments act as preferred pathways for water and solute transport. Fissures are surface features, or gulleys, that are underlain by fractures filled with loose sediment washed in from surrounding areas.

Hydraulic and chemical approaches were used to investigate unsaturated flow processes beneath and adjacent to fissures, and the results were compared with data from surrounding geomorphic systems such as arroyos, ephemeral streams, and interstreams. Typically, high water potentials in surficial sediments result from infiltration of recent precipitation. Below this surficial zone of high water potentials lies a zone of low water potentials that is much thinner beneath the fissure than in adjacent sediments or in sediments beneath ephemeral streams and interstreams. Maximum chloride concentrations in profiles in the fissured sediments (80 to 105 g m^{-3}) were much lower than those measured in all other geomorphic systems (2,000 to 6,000 g m^{-3}) because chloride is leached in the vicinity of the fissures. Minimum estimates of the moisture flux from chloride data ranged from 1 to 8 mm yr^{-1} in the fissured sediments and were up to 350 times greater than those calculated for ephemeral stream and interstream settings. The corresponding moisture velocities in the fissured sediments ranged from 10 to 70 mm yr^{-1}. A tracer experiment demonstrated higher downward water and solute transport in the fracture fill beneath the fissure relative to adjacent sediments. Numerical simulations of the tracer experiment with the computer code TRACR3D reproduced the overall shape of the tracer plume. Sensitivity analyses demonstrated that the tracer plume is most sensitive to spatial variability in soil texture and the corresponding hydraulic parameters. The results from this study suggest that sediments in the fissured area act as preferred pathways because surface runoff is concentrated in the fissures and because underlying fractures and cavities provide avenues for rapid moisture and solute transport. Comparisons of moisture fluxes in fissured

---

sediments in this system with fluxes in preferred pathways in other arid regions indicate that the primary controls on percolation rates are the duration of inundation and the presence of subsurface structures such as fractures or sinkholes that allow rapid water and solute movement.

INTRODUCTION

Although moisture flux in the unsaturated zone of arid regions has generally been considered negligible, recent work related to radioactive waste disposal indicates that this is not true in all arid systems (Gee and Hillel, 1988). Previous studies have shown large local variations in moisture flux as a result of enhanced percolation along preferred flow paths such as arroyos, playas, and karstic sinkholes (Allison et al., 1985; Tyler et al., 1986; Stone, 1990). Surface runoff is focused in these geomorphic systems, and depending on the subsurface soil texture, deeper percolation may occur relative to that in surrounding areas. These preferred flow paths correspond to "macroscopic scale" flow paths discussed by Gee and Hillel (1988). Large variability in moisture flux between different geomorphic systems underscores the importance of determining moisture flux in each of these systems to estimate areal recharge and to characterize sites for waste disposal. Much higher percolation rates along preferred flow paths more readily transport contaminants and bypass much of the unsaturated zone.

The objective of this study was to determine if fissured sediments act as preferred pathways for unsaturated water and solute movement in the Chihuahuan Desert of Texas. Key components of this research include determination of moisture flux in the unsaturated zone beneath fissures and comparison with that in previously studied unsaturated sediments beneath arroyos, ephemeral streams, and interstreams within this study area. Data from hydraulic and chemical approaches should complement each other and provide a more comprehensive conceptual model of unsaturated flow processes in this system. Hydraulic methods included monitoring moisture content and measuring water potential. Moisture content is discontinuous across different soil textures; therefore, variations in moisture content with depth cannot be used to determine the direction of water movement. Temporal variations in moisture content are used to detect the movement of water pulses through the system. Under equilibrium conditions, water potential is continuous across different soil textures, and water potential data provide information to assess the direction of the driving force for liquid water movement.

In contrast to the hydraulic methods, which provide information on moisture flux for the duration of the monitoring period, chemical methods provide data on both short- and long-term moisture flux. A tracer test was conducted to obtain

detailed information on moisture flux in the fracture fill beneath a surface fissure and in adjacent sediments. Numerical simulations of the tracer experiment with the computer code TRACR3D were used to evaluate controls on flow and transport. The chloride mass balance approach was used to calculate long-term net moisture fluxes in this setting.

Site description

The study area lies in the Hueco Bolson, a sediment-filled basin within the Chihuahuan Desert of Texas in the eastern portion of the Basin and Range structural province (Fig. 1). A "bolson" is a closed basin with centripetal drainage. The sediments in the Hueco Bolson are approximately 200 m thick in the study area and consist of 140 m of clay interbedded with silt and sand of the Tertiary Fort Hancock Formation, overlain by up to 15 m of predominantly coarse-grained material of the Tertiary—Quaternary Camp Rice Formation. These clastic sediments were washed in from adjacent mountains. Cretaceous and older rocks are exposed on the Diablo Plateau north and east of the study area.

Four primary geomorphic systems were recognized in the study area: ephemeral streams and interstreams, arroyos, and fissures (R.W. Baumgardner, pers. commun., 1989). Ephemeral streams lack well-defined channels (maximum relief of 0.6 m) and drain into arroyos. Absence of incised channels throughout much of the study area indicates that sheet flow constitutes a major portion of surface runoff. Interstream areas are topographically higher and contain dunes in some areas. Arroyos border the study area and drain into the Rio Grande. The topographic expression in the arroyos is at least 50 times that in the ephemeral streams. Arroyos are incised through the Camp Rice Formation, and arroyo floors consist of a thin layer of gravel ($\leq$ 2 m) that overlies the clay-rich Fort Hancock Formation (R.W. Baumgardner, pers. commun., 1990). The streams and arroyos are generally dry except after precipitation.

Fissures in the study area are described in detail by Baumgardner and Scanlon (in press), and only a brief summary of those features related to unsaturated zone hydrology are presented in this paper. The term *fissure* refers to the alignment of discontinuous surface collapse structures, or gulleys; the underlying extensional feature, called a fracture, is filled with sediment. Three fissures were mapped in the study area (Fig. 1). The longest fissure in the study area (fissure # 1) formed between 1971 and 1985 and the other two fissures formed after 1989. The surface collapse features are as much as 1.4 m deep by 1.6 m wide. Trenches excavated at right angles to one of the fissures show that the fracture width ranges from 65 mm at 3.8-m depth to 25 mm at 5.6-m depth. The maximum vertical extent of
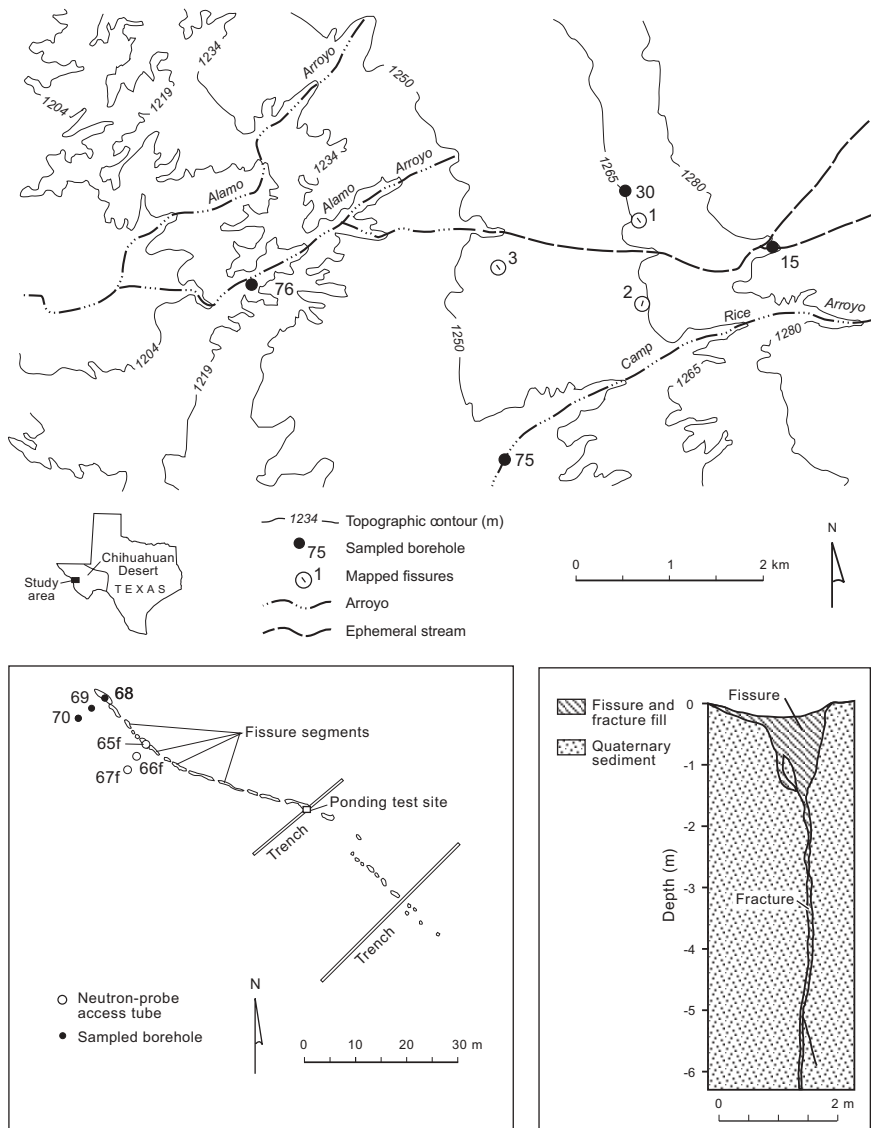
Fig. 1. Location of sampled boreholes. Three fissure locations are labeled 1, 2, and 3. (a) Plan view of fissure no. 1 and location of sampled boreholes, neutron-probe access tubes, and ponding test and (b) cross section of fissure no. 1 at the ponding test site are shown in the insets. [QA16585c]

the fracture is unknown because none of the trenches reached the base of the fracture. The fractures are filled with loose sediment that has similar texture to adjacent sediments. Soil texture is highly variable and ranges from clay loam to clast-supported gravel ($\leq$ 80% gravel). Some zones are strongly cemented with $CaCO_3$. Open cavities exposed in trench walls are generally less than 0.1 m in width and may result from collapse material being dispersed in the clast supported gravels, or from animals as suggested by rodent fecal pellets (Baumgardner and Scanlon, in press.). The strata are sufficiently cohesive for cavities to remain open. Plant roots have been found in the fracture fill down to 5-m depth and probably reflect the looser texture of the soil that has been washed in to fill the fracture.

Fissure development in the study area is thought to follow the model proposed by Larson and Pewe (1986) (Baumgardner and Scanlon, in press.). Tension fractures in the shallow subsurface are enlarged by erosion, which forms horizontal soil pipes. Sediment collapses into the pipes. The resulting surface collapse features occur in local topographic lows perpendicular to drainage and act as sinks capturing runoff from surrounding sediments as indicated by washed-in leaf litter. Elongation and lateral connection of surface collapse features forms fissures. Although fissure development in Arizona has been attributed to differential compaction of sediments related to groundwater withdrawal (Jachens and Holzer, 1979), groundwater production in this portion of the Hueco Bolson has been minimal. Lowering of base level related to the incision of the Rio Grande in the Hueco Bolson (Mullican and Senger, in press) may have caused natural groundwater level declines that could have resulted in the development of fissures. Various hypotheses related to geologic controls on fissure development are examined in Baumgardner and Scanlon (in press).

METHODS

Information on many of the procedures used in this study can be found in Scanlon (in press) and in Scanlon et al. (1991), and only those methods not previously discussed are described here in detail. Soil samples were collected from three boreholes (68, 69, and 70); borehole 68 was drilled in the fissure, and boreholes 69 and 70 were drilled at distances of 3 and 6 m, respectively, at right angles to the general trend of the fissure (Fig. 1). Soil samples collected from these boreholes were analyzed for soil texture, gravimetric moisture content, and water potential. Soil texture was classified according to Folk (1974) in samples that contained gravel and according to the U.S. Department of Agriculture (1975) in samples that did not contain gravel. Total (matric + osmotic + gravitational)

potentials are generally used to estimate the direction of the driving force for water movement. Matric potential results from capillary and adsorptive forces and osmotic potential results from chemical concentration gradients. Matric and osmotic potential constitute water potential, which was measured in the laboratory with a Decagon® psychrometer sample changer. The osmotic component (ψ_π) of water potential was estimated from chloride concentration of soil water according to the van't Hoff equation (Campbell, 1985):

$$\psi_\pi = (\nu C\chi\ RT)/1000 \tag{1}$$

where ν is number of osmotically active particles (2 for NaCl); C is concentration (moles kg^{-1}); χ is osmotic coefficient (Robinson and Stokes, 1959); R is gas constant (8.3142 J mole^{-1} °K^{-1}); and T is temperature (°K). The gravitational potential was calculated from the elevation above the water table. In addition to laboratory measurements, moisture content was monitored in the field in three neutron-probe access tubes (65f, 66f, and 67f) that were installed parallel to the three boreholes (Fig. 1). Moisture content was logged approximately monthly at 0.1-m intervals from a depth of 0.3 to 6 m from October 1989 to March 1990.

Chemical methods included analysis of chloride concentrations in soil-water extracts from samples collected in boreholes 68, 69, and 70 to estimate moisture flux through the unsaturated zone. Chloride concentrations are inversely proportional to moisture flux; high chloride concentrations reflect low moisture fluxes because chloride, which is nonvolatile, is concentrated by evapotranspiration, whereas low chloride concentrations indicate high moisture fluxes because chloride is leached. The volumetric moisture flux for depth interval i (q_{wi}) is calculated according to the following equation:

$$q_{wi} = J_S\ /\ Cl_i \tag{2}$$

where J_s is the chloride flux into the soil and Cl_i is the soil-water chloride concentration measured in depth interval i. In areas of negligible surface runoff, J_s is approximated by the mean annual precipitation rate times the chloride concentration in precipitation and in dry fallout (Sharma and Hughes, 1985; Mattick et al., 1987). The mean annual precipitation rate for the study area is 280 mm yr^{-1} (J. Griffiths, pers. commun., 1990). The mean chloride concentration (Cl_p: 0.29 g m^{-3}) was calculated from the prebomb $^{36}Cl/Cl$ ratio (0.46×10^{-12}) measured in soil water from a borehole approximately 0.5 km from the fissure, and the natural ^{36}Cl fallout at the site estimated as 20 atoms ^{36}Cl m^{-2} s^{-1} (Bentley et al., 1986; Scanlon (in press)). The resultant J_s value was 0.08 g m^{-2} yr^{-1}. The travel time (t) represented by chloride in the depth interval z_i can be evaluated by dividing the total mass of chloride from the surface to that depth by the chloride flux:

$$t = \Sigma\ Cl_i\ z_i\ /\ J_s \tag{3}$$

Fig. 2 Location of fracture and five sampling profiles parallel to fracture beneath ponded surface. The strata are of fine-grained material at the ponded surface, underlain by gravel, a petrocalcic layer (light-colored), fine sediment, and gravel at the base.

Although surface "runon" occurs into the fissures (Baumgardner and Scanlon, in press), discharge rates and chloride concentrations of runon were not quantified. As a result, moisture fluxes calculated according to eqn. (2) provide a lower limit of the actual moisture flux in the unsaturated zone beneath the fissures because the contribution of chloride from runon was neglected. Hydrodynamic dispersion is not represented in eqn. (2); however, inaccuracies in moisture fluxes that result from neglecting hydrodynamic dispersion should be much less than those that result from omitting chloride input from surface runon. The moisture flux is divided by the volumetric moisture content to obtain the moisture velocity (q_W/θ), which represents the actual rate of solute transport.

A tracer experiment was conducted to evaluate moisture and solute movement in the sediment-filled fracture relative to adjacent sediments. The test was conducted in a trench (Fig. 1) that had been excavated to a depth of approximately 4 m at right angles to the trend of the fissure (Fig. 2). A 4-m^2 area was ponded to an average depth of 0.4 m for approximately 6 h. The ponding depth was based on the estimated flood depth that would result from a 100-yr precipitation event in this area using HEC1 and HEC2 (U. S. Army Corps of Engineers, 1981, 1982) computer codes (S. Akhter, pers. commun., 1991). The fracture was located in the center of the ponded area. Bromide was selected as a tracer because it is

chemically conservative and background concentrations in interstitial water are zero. Water for the ponding test was obtained from a nearby well and had a naturally high chloride concentration (240 g m^{-3}); bromide was added to the water at a concentration of 330 g m^{-3}. The walls of the ponded area consisted of natural sediment, and lateral flow of water from the pond was allowed. The ponding site was not instrumented with neutron-probe access tubes or soil solution samplers to avoid introducing artificial pathways for the ponded solution. After ponding ended, the ponded area was excavated with a bulldozer to a depth of 2.2 m below the ponded surface. Approximately 50 soil samples were collected at depth intervals of 0.2 to 0.4 m in the fracture fill and along five profiles at distances of 0.2, 0.5, 1.0, 1.5, and 2 m parallel to the fracture fill (Fig. 2). These soil samples were analyzed for texture and moisture content. Soil-water extracts from these samples were analyzed for chloride concentration by titration and for bromide concentration by ion chromatography. Because the flow meter malfunctioned during the 6 h ponding, an accurate measurement of the amount of infiltrated water could not be made; therefore, mass balance for the experiment could not be calculated. Even if the amount of infiltrated water were known, the accuracy of mass balance calculations would be questionable because the experiment was three dimensional and subsurface sampling was restricted to two dimensions. Extrapolation of the two-dimensional data to three dimensions is unrealistic because of the extreme heterogeneity of soil textures.

    The tracer experiment was simulated with the advection dispersion equation (Biggar and Nielsen, 1967). Assumptions associated with the advection dispersion equation include a homogeneous medium and lateral mixing of solutes normal to the mean flow direction. Although the assumption of soil homogeneity is not valid at this site, horizontal stratification of the soil may allow lateral mixing of the solutes. Because of soil heterogeneity and the existence of fractures, an alternative process model such as the stochastic advective model (Dagan and Bresler, 1979; Jury and Roth, 1990) may represent the transport processes more accurately, particularly near the surface and in the fractures. According to this stochastic model, solute moving in isolated stream tubes at different velocities has insufficient time to mix with that in adjacent stream tubes. In the stochastic model, the dispersion coefficient increases linearly with time, whereas with the advection dispersion equation or Fickian model, the dispersion coefficient increases with the square root of time. There is insufficient information for this ponding experiment to determine which model is most applicable.

    The tracer experiment was simulated with the computer code TRACR3D (Travis and Birdsell, 1991). The TRACR3D code solves three-dimensional, isothermal, transient, two-phase flow and multicomponent transport in variably saturated porous media. An implicit finite-difference scheme is used to solve the flow and

transport equations. Previous attempts to use other codes such as UNSAT2 (Davis and Neuman, 1983), TRUST (Narasimhan et al., 1978) and FEMWATER (Yeh and Ward, 1979) to solve the flow equation for infiltration into dry soil (ψ < -0.1 MPa) resulted in convergence problems. TRACR3D includes many features that enhance its ability to converge for highly nonlinear flow problems such as use of the Newton-Raphson iterative scheme, which is more strongly convergent (second order) than the generally used Picard scheme (first order). An efficient, preconditioned, conjugate gradient method is used to solve the asymmetric matrices at each iteration. TRACR3D uses a variable time-stepping scheme that is based on the number of iterations per time step. Solution of highly nonlinear flow problems is sensitive to the time-stepping scheme because the time step may vary by many orders of magnitude. The governing mass conservation equations for liquid (4) and tracer (5), and momentum conservation equation for liquid (6) are given by the following:

$$\partial_t(\phi \, \sigma \, \rho) + \nabla \cdot \left(\rho \, \vec{u}\right) = 0 \tag{4}$$

$$\partial_t(\phi \, \sigma \, \rho \, C) + \nabla \cdot \left(\rho \, \vec{u} \, C\right) = \nabla \cdot \left(\phi \, \sigma \, D \, \rho \, \nabla C\right) \tag{5}$$

$$\vec{u} = \left(\frac{k_r \, k_s}{\mu}\right) (\nabla P + \rho \hat{g}) \tag{6}$$

where ϕ is porosity, σ is saturation, ρ is fluid density, u is fluid velocity, C is tracer concentration, D is dispersivity tensor, k_r is relative permeability, k_s is saturated permeability, μ is fluid viscosity, P is liquid pressure, and g is gravitational acceleration. The above equations describe advective-dispersive transport of the tracer. Molecular diffusion was neglected because high flow velocities during ponding should cause mechanical dispersion to be much greater than molecular diffusion. Neglecting sorption is justified because chloride and bromide are chemically conservative. Information on dispersivity was not available for these sediments, and sensitivity analyses were conducted to determine the effect of varying dispersivity from 0 to 100 mm, which is within the range of observed laboratory and field dispersivities (Schulin et al., 1987a, 1987b; Wierenga and Van Genuchten, 1989). Values of initial water potentials and tracer concentrations were based on measurements of these parameters in soil samples from similar depth intervals in nearby boreholes 68, 69, and 70. The upper boundary was specified as a constant head (0.4 m) equal to that used in ponding. The lower boundary condition was fixed at ambient water potential, and continuative tracer outflow was allowed. Zero fluxes were assigned to the left boundary as a result of symmetry and also to the right boundary. The width of the grid (2.2 m) was chosen to minimize the effect of the right boundary condition on movement of
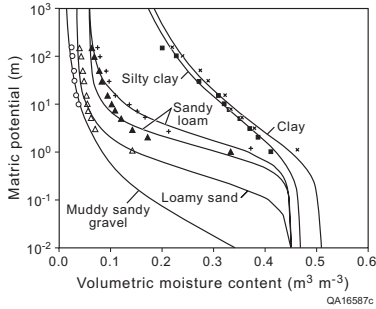
Fig. 3. Retention curves for different soil textures. Points represent measured matric potentials and moisture contents, and lines represent fitted retention curves based on van Genuchten (1980). [QA16587c]

the wetting front. The modeled cross section was discretized into approximately 2,600 cells, and nodal spacing ranged from 10 mm in the fracture fill to 50 mm in adjacent sediments. Spatial variability in material properties was based on laboratory-measured moisture retention and saturated hydraulic conductivity (K_S) data of soil samples collected nearby (Fig. 3) (Scanlon et al., 1991) that had similar textures to those observed beneath the ponded surface. These material properties are approximate because of differences in soil texture between the ponded sediments and those for which material properties were measured. The differences in texture were greatest in the coarse-grained sediments. Gravel content in the ponded sediments was $\leq$ 80%, whereas gravel in the sample for which K_S and moisture retention were measured was 30%. The saturated hydraulic conductivity of the fracture fill was not measured because of the difficulty of collecting undisturbed soil samples from loose sediment within the 30- to 50-mm fracture width that contained some open cavities. The following analytical function (Van Genuchten, 1980) was used to describe the θ/ψ relationship for different soil textures (Fig. 3; Scanlon et al., 1991):

$$\theta = \theta_r + \frac{\theta_s - \theta_r}{\left[1 + (\alpha\,\psi_m)^n\right]^m} \tag{7}$$

where θ_r is residual water content, θ_s is saturated water content, ψ_m is matric potential, and α, n, and m are empirical parameters. The computer program RETC (Van Genuchten, 1985) was used to obtain estimates of the fitting parameters (α and n). The unsaturated hydraulic conductivity was calculated from the fitted soil-water-retention functions and the measured K_S data using Mualem's model (Mualem, 1976) and by restricting m to 1–1/n (Van Genuchten, 1980):

$$K_u(\psi) = \left(\frac{\left\{1 + (\alpha\,\psi_m)^{n-1}\left[1 + (\alpha\,\psi_m)^n\right]^{-m}\right\}^2}{\left[1 + (\alpha\,\psi_m)^n\right]^{m/2}}\right) K_S \tag{8}$$
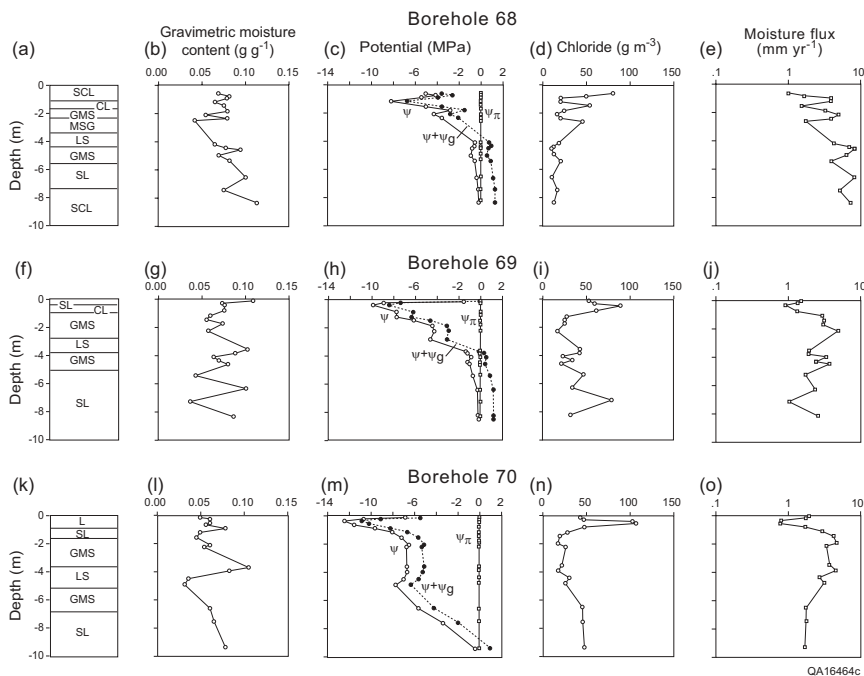
Fig. 4. Profiles of soil texture, gravimetric moisture content, water potential (y), osmotic potential (yp), total potential (y+ yg), chloride concentration, and calculated moisture flux for boreholes 68, 69, and 70. Soil textures include muddy sandy gravel (msg), gravelly muddy sand (gms), loamy sand (ls), sandy loam (sl), sandy clay loam (scl), loam (l), and clay loam (cl). For location of boreholes, see Fig. 1. [QA16464c]

RESULTS AND DISCUSSION

Soil texture in samples from boreholes 68, 69, and 70 ranged from clay loam to muddy sandy gravel (Fig. 4a, f, and k). Moisture content showed no systematic variation with depth and ranged from 0.03 to 0.11 g g^{-1} (Fig. 4b, g, and l). Soil texture and moisture content in samples collected from the profile beneath the fissure (Fig. 4a and b) were similar to those in adjacent profiles (Fig. 4f, g, k, and l). Monthly monitoring of moisture content from October 1989 through March 1990 in access tubes located in the fissure (Fig. 5a) and in adjacent sediments (Figs. 5b and c) showed that moisture content remained constant within the limitations of the neutron probe measurements (standard error of calibration equation ± 0.01 m^3 m^{-3}), although precipitation events up to 6 mm and runoff were recorded
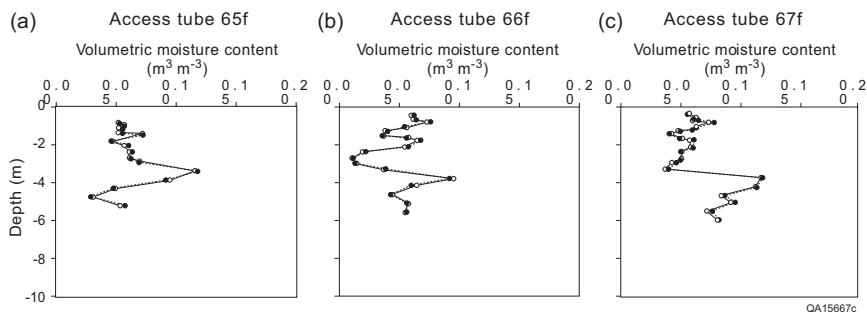
Fig. 5. Variation in volumetric moisture content with depth and time in access tubes (a) 65f, (b) 66f, and (c) 67f. Water content was monitored monthly from October 1989 through March 1990, at 0.1-m intervals from 0.3 m to total depth, and five curves are represented. For location of access tubes, see Fig. 1. [QA15667c]

during this time. The shallowest depth monitored by the neutron probe was 0.3 m; therefore, infiltration events restricted to shallower depths would not be detected by neutron logging. Because a constant flux could result in temporally invariant moisture content, the absence of variations in moisture content does not preclude downward water movement.

In dry soils, water potential is a much more sensitive indicator of soil water dynamics than moisture content because variations in water potential are much greater than variations in moisture content in the dry range, as reflected by the shape of the moisture retention curves (Fig. 3). All three water potential (ψ) profiles in the fissured area displayed similar trends (Fig. 4c, h, and m): moderately high water potentials at the surface, which decreased to a minimum at depths of 0.4 to 0.7 m and increased to a maximum at depths of ≥ 4 m (Fig. 4c) beneath the fissure to ≥ 9 m (Fig. 4m) in the profile 6 m from the fissure. Boreholes 68, 69, and 70 were drilled and sampled within 3 consecutive days; however, a precipitation event affected water potentials in samples collected from the shallowest depth (0.1 m) and resulted in much higher water potentials in the uppermost sample from borehole 69 (Fig. 4h; ψ: -1.5 MPa), which was collected immediately after the precipitation event relative to samples from the same depth in borehole 68 (Fig. 4c; ψ: -5 MPa) collected before precipitation and in borehole 70 (Fig. 4m; ψ: -7 MPa) collected after precipitation. The minimum water potential decreased away from the fissure (borehole 68: ψ: -8 MPa; borehole 70: ψ: -12 MPa), and the zone of low water potentials increased away from the fissure (Fig. 4c, h, and m). High water potentials (-0. -0.4 MPa) were measured in soil samples from the base of these profiles. The osmotic component of water potential was negligible
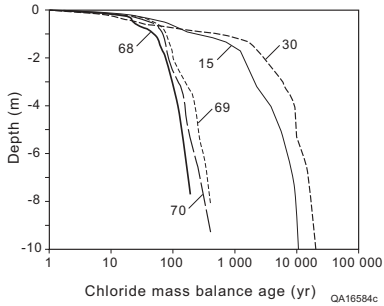
Fig. 6. Chloride mass balance age calculated according to eqn. (2). Borehole numbers shown adjacent to each line. Boreholes 68, 69, and 70 were drilled in the fissured sediments; borehole 15 in an ephemeral stream, and borehole 30 in an interstream setting. For location of boreholes, see Fig. 1.[QA16584c]

($\psi_\pi \geq$ -0.01 MPa), and variations in gravitational potential were very small (0.1 MPa); therefore, water potential (ψ) approximates total potential ($\psi + \psi_g$) and can be used to assess the direction of the driving force for water movement. Downward water potential gradients in the surficial sediments reflect infiltration of recent precipitation. Below this surficial zone, upward water potential gradients suggest an upward driving force for water movement controlled by evapotranspiration.

The hydraulic data described above reflect a limited period—1 day in the case of the water potential data and 6 months in the case of the moisture content monitored with the neutron probe. Because of the limited monitoring period, the hydraulic data provide only a snapshot of unsaturated flow processes in this system. In addition, these data represent infiltration and evapotranspiration events that occurred during the sampling and monitoring period and not the net water movement. In contrast, chloride concentration data provide information on net water movement over long periods. The environmental chloride profile beneath the fissure (borehole 68) is characterized by low concentrations (Fig. 4d; 10 to 80 g m^{-3}), similar to concentrations of chloride in adjacent profiles from boreholes 69 (Fig. 4i; 17 to 90 g m^{-3}) and 70 (Fig. 4n; 18 to 105 g m^{-3}). The similarity in the range of chloride concentrations among all three profiles indicates that long-term percolation rates are similar in a broad zone parallel to the fissure. Calculated moisture fluxes ranged from 1 to 8 mm yr^{-1} (Fig. 4e, j, and o), and moisture velocities ranged from 10 to 70 mm yr^{-1}. Maximum moisture fluxes decreased from 8 mm yr^{-1} beneath the fissure (borehole 68) to 5 mm yr^{-1} in adjacent sediments (boreholes 69 and 70). Travel times calculated according to eqn. (3) ranged from 0 to 420 yr (Fig. 6). Calculated moisture fluxes represent a lower limit of the actual moisture flux and travel times represent an upper limit because chloride input from runon into the fissure was neglected.
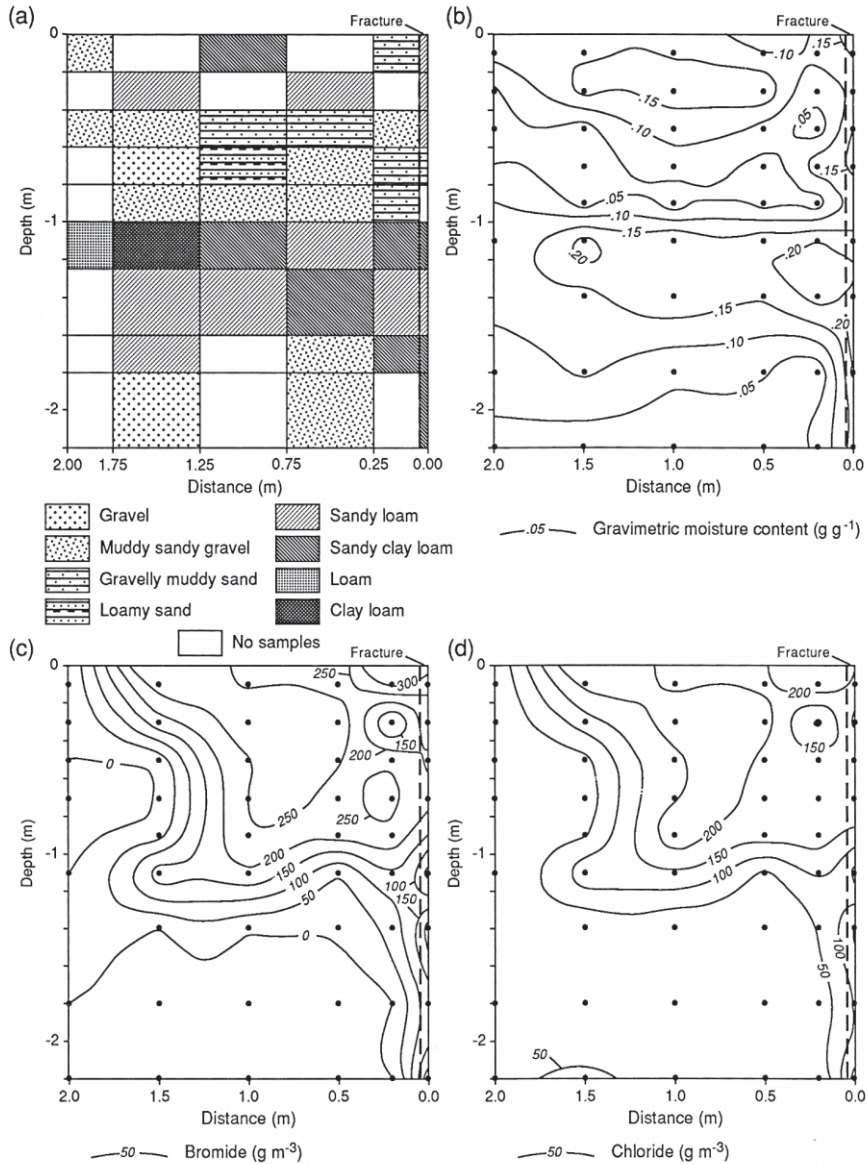
Fig. 7. Cross section of (a) sediment texture, (b) gravimetric moisture content, (c) contoured bromide and (d) chloride concentrations in soil samples collected beneath the ponded surface. [QA15669c]
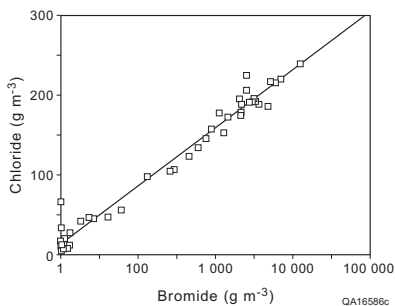
Fig. 8. Relationship between chloride and bromide concentrations in water extracts of soil samples collected after ponding ceased. [QA16586c]

Tracer test

Soil texture beneath the ponded area was predominantly coarse grained and ranged from clay loam to gravel (Figs. 2 and 7a). No systematic difference was found between soil texture in the fracture fill and that in adjacent sediments. Gravimetric moisture content after the infiltration test was generally high throughout the sampled zone of the fracture fill and ranged from 0.12 to 0.21 g g^{-1} (Fig. 7b). Variations in moisture content were negatively correlated with percent gravel and sand and positively correlated with percent silt and clay. These correlations were statistically significant at α of 0.05. Zones of low moisture content (0.03 to 0.04 g g^{-1}) at a depth of 0.6 to 1.0 m below the ponded surface corresponded to a gravel-rich layer. The observed large variations in moisture content with differences in soil texture make it difficult to discern the position of the wetting front from moisture content data alone.

Soil-water bromide concentrations were high in the fracture fill to a depth of 2.2 m, whereas bromide concentrations were close to background values at a depth of 1.4 m in adjacent sediments (Fig. 7c). The tracer front adjacent to the fracture was sharp, and the shape of the front was relatively smooth. The distribution of the tracer showed significant horizontal movement as evidenced by high bromide concentrations 1.5 m from the fracture, although the ponded surface only extended 1 m from the fracture. The profile at 2 m from the fracture had no bromide. Bromide data indicate that the lateral extent of the wetted zone is restricted in the gravel-rich layer at a depth of 0.6 to 1.0 m. The distribution of chloride is similar to bromide ($r^2 = 0.98$), with the exception that background chloride concentrations are not zero (Figs. 7d and 8). The chemical tracer data show that water flowed preferentially in the fracture fill relative to the surrounding sediments. The excavation depth of 2.2 m below the ponded surface was insufficient to reach the base of the wetting front in the fracture fill; however, the

TABLE 1

Summary of sensitivity analyses and related CPU time.

Attribute	Lower bound		Nominal case		Upper bound	
	Variable (h)	CPU time	Variable (h)	CPU time	Variable (h)	CPU time
Grid size (mm)			50	7.0	100	1.0
Soil texture	uniform silty clay	0.3	nonuniform clay to gravel	7.0	uniform sandy loam	9.0
Initial water potential (MPa)	–2.0	8.0	–1.0	7.0	–0.1	5.0
Dispersivity (mm)	0.0	7.2	10	7.0	100	7.3
Ponding depth (mm)	0.1	7.0	400	7.0	800	7.0

wetting front only penetrated to a depth of approximately 1.4 m in the adjacent material.

Numerical simulations

The purpose of the modeling study was not to reproduce the exact distribution of the tracers, given the complexity of the flow system, the difficulty of representing cavities, and the lack of data. Instead, the primary objective of the exercise was to use the model as a tool to evaluate quantitatively the effect of variations in hydraulic parameters on the movement of tracers in this system. The nominal case consisted of initial water potentials of -1.0 MPa (Table 1) that were based on data from nearby borehole 68. Initial chloride concentrations of 10 g m^{-3} were also based on data from nearby boreholes, and initial bromide concentrations were 0 g m^{-3}. The ponding boundary condition, dry initial conditions, and soil heterogeneities that had large conductivity contrasts made this problem computationally difficult. The CPU time on a MicroVax computer work station was approximately 7 h (Table 1), which is slightly longer than the duration of the ponding experiment (6 h). Cumulative mass balance errors on fluid and tracers were less than 1 part in 10^6 for all simulations.

The simulation results were evaluated by comparing predicted (Fig. 9a) and observed (Fig. 9b) bromide concentrations because the plume is most clearly shown by bromide (Fig. 9a). Saturated hydraulic conductivity of the fracture-fill sediments was increased by a factor of 10 relative to that of similar textures in adjacent sediments to obtain good agreement between observed and simulated tracer concentrations in the fracture fill. The water potential data showed that the core of the moisture plume was saturated after 6 h of ponding (Fig. 9b). The core
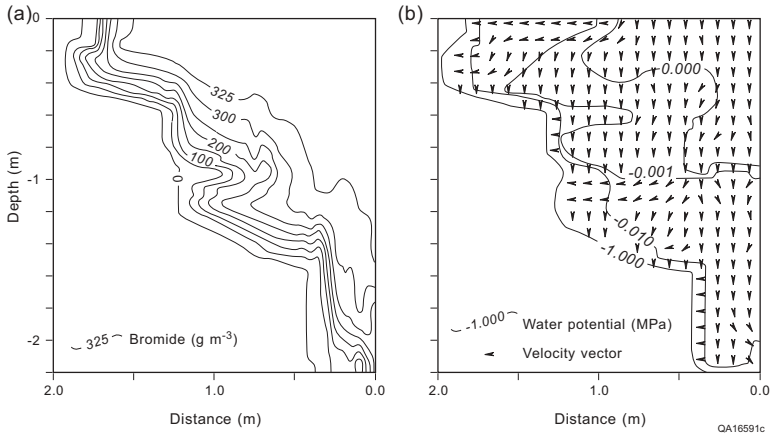
Fig. 9. Results of numerical simulations: (a) contoured plot of bromide concentrations, (b) water potentials (MPa), and velocity vectors. Because of the large range in velocities, all vectors were plotted with uniform length. [QA16591c]

of the plume (ψ = 0.000 MPa) is dominated by gravitational flow, whereas the fringe (ψ = -1.000 MPa) of the plume is dominated by capillary effects. Velocity vectors generally plot at right angles to the water potential contours and are vertical in the core of the plume where gravitational flow is dominant and vary from vertical to horizontal in the fringe of the plume. Moisture flux in the core of the
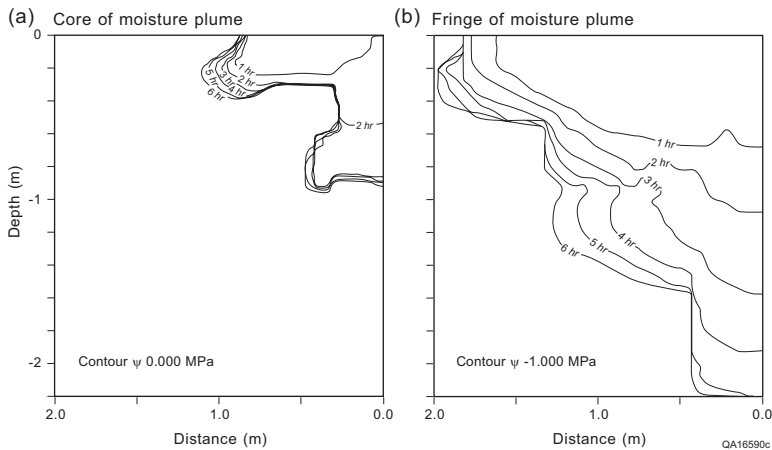

Fig. 10. Evolution of (a) the core (y = 0.000 MPa) and (b) the fringe (y = -1.000 MPa) of the moisture plume with time (hours). [QA16590c]

plume is approximated by the saturated hydraulic conductivity of the sediments and is retarded in the vertical direction by the low saturated hydraulic conductivity of loam sediments (Figs. 7a and 10a). In contrast, migration of the fringe is dominated by capillary effects and is impeded in vertical and lateral directions by the low unsaturated hydraulic conductivity of coarse gravel sediments (Figs. 7a and 10b).

Numerical simulations generally reproduced the overall bromide plume shape with similar tracer front depths and restricted lateral flow in the gravel zone at depths of 0.6 to 1.0 m (Fig. 9a). Although the computer simulation predicted increased lateral spreading below the gravel layer (Fig. 9a), the amount of lateral spreading is much less than that observed (Fig. 7c). The reduced spreading of the simulated plume relative to that of the observed plume below the gravel may be attributed to insufficient information on the soil textural distribution and the approximate nature of the material properties assigned to these textures. In the core of the plume, simulated tracer concentrations (Fig. 9a) were uniformly high and equal to the tracer concentration in the input water (330 g m^{-3}), whereas observed tracer concentrations were spatially variable and ranged from 100 to 300 g m^{-3} (Fig. 7c). These discrepancies between observed and predicted tracer concentrations are difficult to reconcile. Temporal variations in input concentrations cannot account for the lower observed concentrations because tracer concentrations in the ponded water varied less than 1%. Any drying during exposure of the trench wall would increase rather than decrease the tracer concentration. Errors in gravimetric moisture content, particularly in coarse-grained samples, as a result of small sample size would alter the volumetric tracer concentration; however, contour plots of gravimetric chloride and bromide concentrations (grams per kilogram of dry soil) were similar to those of volumetric concentrations. Nonuniform solute transport and mixing of mobile and immobile water may account for the reduced observed concentrations. Nonuniform transport could result from preferential flow in root channels or fractures (Germann, 1988) and/or along unstable wetting fronts where fine-grained sediments overlie coarser sediments (Glass et al., 1988). The apparent smoothness of the observed plume front does not seem to support the nonuniform solute transport hypothesis; however, this smoothness may be an artifact of low sample density relative to the scale of the preferential flow pathways. Information on the evolution of the plume as the tracers migrate through the different sediment layers and more detailed characterization of the tracer front would be required to evaluate the importance of nonuniform solute transport.

Sensitivity analyses were conducted to determine the effect of varying selected parameters on the distribution of the tracers (Table 1). Differences in the CPU time required for the various simulations also provide some insight into the
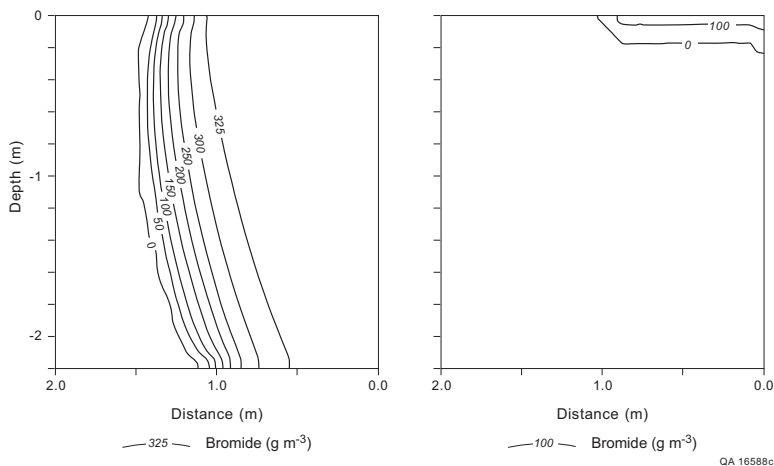
Fig. 11. Bromide concentrations that result from infiltration into (a) uniform sandy loam and (b) uniform silty clay. [QA16588c]

numerical difficulties of the simulations. Approximately doubling the grid size resulted in smearing of the solute front, and the resultant concentration gradients were reduced by up to 30%. This increase in the grid size corresponded to a decrease in the number of nodes from approximately 2,600 to approximately 800 and in the CPU time by 86% (Table 1). Attempts to simulate a grid size reduced by approximately 50% were abandoned because estimated CPU time would be approximately 100 h. Model output was most sensitive to the representation of the soil type. The distribution of the tracers is markedly different when the soil is represented by uniform sandy loam (Fig. 11a) or uniform silty clay (Fig. 11b). The CPU time was increased to 29% when the soil was represented by uniform sandy loam and was decreased by 96% when the soil was represented by uniform silty clay.

The distribution of the tracers was unaffected by variations in water potential within the range of -0.1 to -2 MPa. The minimal effect of these initial water potentials is attributed to the shape of the retention curves, which shows negligible differences in water content corresponding to large variations in water potential except at very high water potentials (Fig. 3). Reducing the initial water potential by a factor of 10 from -1 to -0.1 MPa reduced the CPU time by 29%, whereas doubling the initial water potential increased the CPU time by 14%. Variations in dispersivity from 0 to 100 mm resulted in negligible differences in the distribution of the tracer and in the CPU time. Differences in ponding depth from 0.1 to 800 mm did not alter the distribution of the tracers nor vary the CPU time. These results

are consistent with the findings of Philip (1958) which suggest that the effect of ponding depth on wetting front migration decreases as the sediments become drier and also with time as gravitational potential becomes dominant. The lack of sensitivity to this range in ponding depths is attributed to the predominance of capillary effects during the early stages of infiltration into these dry sediments. During this stage,water potentials in the unsaturated zone (-10,000 mm) were much lower than the ponding depths considered (0.1 and 800 mm). During later stages, gravitational forces were dominant, and moisture flux was controlled by the saturated hydraulic conductivity of the sediments and unaffected by ponding depth. Although the ponding test was designed to evaluate percolation that would result from a ponding depth that was based on a 100-yr precipitation event, these simulations suggest that similar wetting front depths would be obtained for ponding depths as shallow as 0.1 mm.

The results of the sensitivity analyses showed that spatial variability in soil texture and the corresponding hydraulic parameters is very important but that information on initial water potentials and boundary head conditions is not critical. The CPU times associated with these simulations suggest that the numerical difficulty increases as the soil heterogeneity or grain size of the sediment increases and as the initial water potentials decrease because the equations become more highly nonlinear.

Comparisons among arroyos, fissures, ephemeral streams, and interstreams

Unsaturated flow data from the fissured sediments were compared with those from surrounding geomorphic systems to determine if flow rates were much higher beneath the fissure and to develop a conceptual flow model for this area. Hydraulic and chemical attributes of sediments beneath ephemeral streams, interstreams, and arroyos are typified by profiles from boreholes 15, 30, and 76, respectively (Figs. 1 and 12; Scanlon, in press; Scanlon et al., 1991). Although soil textures in the fissured area (Fig. 4a) and in the ephemeral stream (Fig. 12a) and interstream (Fig. 12f) areas are similar, cavities and fractures in the fissured sediments give rise to lower bulk densities and looser soil structure as a result of runoff and piping. Soil texture in the fissured area (Fig. 4a) is markedly different from that beneath the arroyos (Fig. 12k) because the clay-rich Fort Hancock Formation in the arroyos is much shallower as a result of incision.

Moisture content in the fissured sediments (Figs. 4b, g, and l; 0.03 to 0.11 g g^{-1}) was similar to that beneath the ephemeral streams (Fig. 12b; 0.02 to 0.14 g g^{-1}) and interstreams (Fig. 12g; 0.02 to 0.11 g g^{-1}). Higher moisture contents in sediments underlying arroyos (Fig. 12l; 0.02 to 0.33 g g^{-1}) relative to those in other geomorphic settings reflect variations in soil texture and degree of inundation.
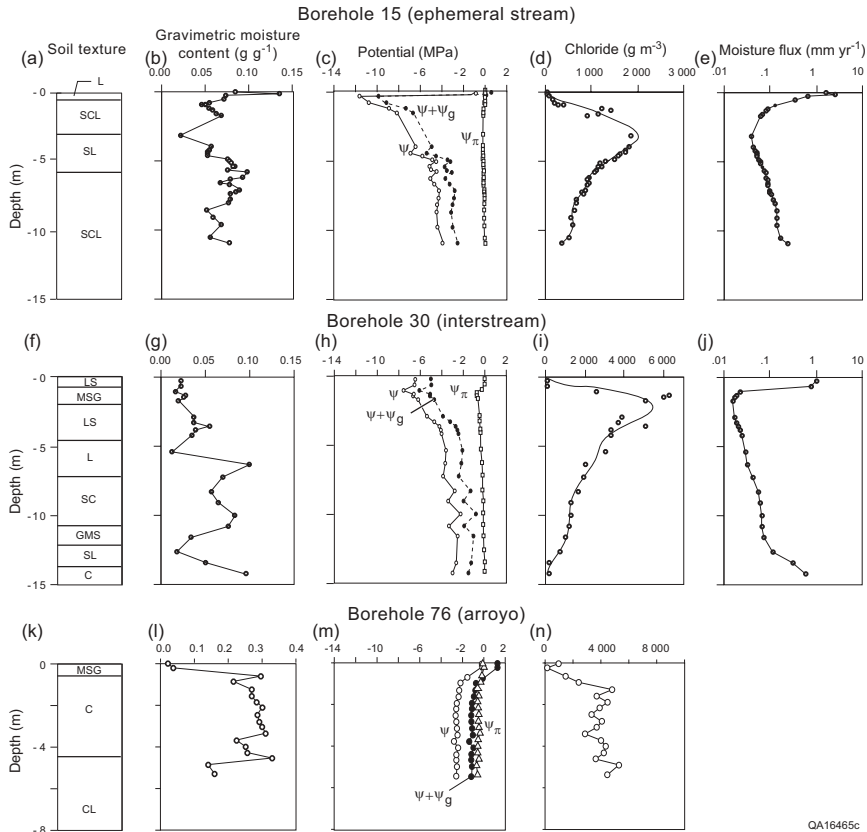
Fig. 12. Profiles of soil texture, gravimetric moisture content, water potential (y), osmotic potential (yp), total potential (y + yg), chloride concentration, and calculated moisture flux for boreholes 15 (ephemeral stream), 30 (interstream), and 76 (arroyo). Soil textures include muddy sandy gravel (msg), gravelly muddy sand (gms), loamy sand (ls), sandy loam (sl), sandy clay loam (scl), loam (l), clay loam (cl), sandy clay (sc), and clay (c). For location of boreholes, see Fig. 1. [QA16465c]

    High water potentials in surficial sediments in many of the geomorphic settings result from infiltration of recent precipitation (Figs. 4c, h, and m, 12c, and m). Below this surficial zone in all geomorphic systems except arroyos, upward water potential gradients indicate an upward driving force for liquid water movement (Figs. 4 and 12). The general shape of the water potential profiles in the fissured sediments (Fig. 4c, h, and m) was similar to those in the ephemeral stream and interstream settings (Fig. 12c and h); however, the zone of low water potentials

was much thinner in the fissured sediments, particularly in the profile directly underlying the fissure (Fig. 4c). Water potentials in soil samples from the base of the profiles in the fissured sediments (-0.2 to -0.4 MPa) were much higher than those from the same depth intervals in profiles beneath ephemeral stream and interstream settings (~ -2 MPa) and indicate that soils near the fissures were wetter than those beneath ephemeral streams and interstreams. Slightly higher water potentials in the interstream profile (Fig. 12h) relative to those in the ephemeral stream profile (Fig. 12c) reflect lower evapotranspiration rates because samples from the interstream profile were collected in midwinter, whereas all other profiles were sampled in midsummer to early fall. Water potentials in arroyo floor sediments (Fig. 12m) were much higher than those in other geomorphic settings, and water potential gradients were low in the arroyo sediments except at the contact between the gravel and clay.

Low chloride concentrations (10 to 105 g m^{-3}) in all three profiles beneath and adjacent to the fissure (Fig. 4d, i, and n) differ markedly from those measured in all other geomorphic settings (Fig. 12d, i, and n). The low concentrations are attributed to leaching of chloride through fractures, cavities, and loosely supported sediment that extend beyond the immediate location of the fissure. The corresponding moisture fluxes in and near the fissures (Fig. 4e, j, and o; 1 to 8 mm yr^{-1}) are up to 350 times greater than those calculated for the same depth interval for the ephemeral stream and interstream settings (Fig. 12e and j). Moisture velocities in the fissured sediments are up to 150 times greater than those in the ephemeral stream and interstream settings. Travel times based on eqn. (2) are much shorter (Fig. 6; 0 to 420 yr) in and near the fissures relative to ephemeral stream and interstream settings (Fig. 6; 0 to 23,000 yr). Because surface runon was neglected in calculations of moisture fluxes, velocities, and travel times in the fissured sediments, differences between actual and calculated values in fissured sediments and in ephemeral stream and interstream sediments may be much greater. There is no systematic difference in moisture fluxes between ephemeral stream and interstream profiles; moisture fluxes in both systems are very low (Scanlon, in press). The shape of the chloride profiles in the fissured sediments is characterized by uniformly low chloride concentrations that contrast with chloride profiles in ephemeral stream and interstream settings. These profiles are characterized by low chloride concentrations in the top meter, as a result of leaching, a gradual increase in concentration to the peak value controlled by evapotranspiration, and a reduction in chloride concentration below the peak, which was attributed to paleoclimatic variation in recharge (Scanlon, in press). High chloride concentrations in clay sediments underlying the arroyos (Fig. 12n; 1,500 to 4,800 g m^3) are attributed to restricted downward water movement in the

clay and high evaporation rates. Moisture fluxes or travel times were not estimated for chloride profiles beneath the arroyos because surface runoff is high and chloride concentrations in runoff were not quantified.

A conceptual flow model was developed for the various geomorphic settings in the Hueco Bolson. Precipitation occurs primarily as high-intensity, convective summer storms and infiltrates to depths of approximately 0.1 to 0.3 m in ephemeral stream and interstream areas. Penetration of moisture is limited by generally fine grain size and low degree of saturation of the surficial sediments. Because most of the moisture is retained in the shallow zone, it is readily evapotranspired. Saturated hydraulic conductivity of the fine-grained sediments is low relative to the high intensity of the precipitation events and results in as much as 50% runoff (S. Akhter, pers. commun., 1989). Runoff from surrounding sediments is captured in fissures and in arroyos because they are topographically lower. Runoff collected in the fissures and surrounding sediments infiltrates readily. Percolation is enhanced by fractures filled with loose sediment and open cavities. This process is reflected in low chloride concentrations in the fissured sediments relative to those in other geomorphic systems. The maximum vertical extent of fractures underlying fissures is unknown; therefore, the depth of increased percolation in the fissured zone relative to surrounding sediments cannot be estimated. Infiltration of runoff in arroyo floor sediments occurs primarily in the gravel sediments and is restricted in the clay section because of the high intensity of the runoff events relative to the low saturated hydraulic conductivity of the clay. Runoff rates are much higher in the arroyos than in all other geomorphic systems because they are topographically lower and because vegetation, which would reduce runoff, is sparse in the arroyos. A saturated zone may develop periodically at the contact between the gravel and clay underlying the arroyos after large runoff events. After runoff ceases, chloride concentrations increase beneath the arroyos as a result of evaporation primarily in the clay because of the greater amounts of water stored in the clay relative to the gravel.

The dynamics of unsaturated flow beneath the different geomorphic systems is reflected in the surface vegetation. Saltcedar (*Tamarix* subsp.) is a phreatophyte and is generally restricted to water courses (Gay and Fritschen, 1979; Davenport et al., 1982). Saltcedar was found in the vicinity of the arroyos in the present study and probably depends on greater amounts of water available in this setting than in other geomorphic systems. Honey mesquite (*Prosopis glandulosa*) is also a phreatophyte, but it has developed mechanisms for tolerating water stress (Nilsen et al., 1984). Honey mesquite is found in the fissured area, ephemeral streams, and interstreams and forms dunes in some parts of interstream settings. Creosote (*Larrea tridentata*) is also widely distributed in the study area and is not

restricted to the watercourses. Creosote can withstand water potentials less than -8 MPa (Odening et al., 1974).

Comparison of recharge rates along preferred flow paths in other regions

Moisture fluxes in the fissured sediments of this study were compared with those along preferred flow paths in other regions to evaluate controls on unsaturated flow and solute transport. Although fissures in the Hueco Bolson would be more directly comparable with fissures in many areas of Arizona (Jachens and Holzer, 1979), unsaturated flow processes in the Arizona fissures have not been studied.

Recharge rates in the Diablo Plateau, northeast of the study area, were based on the presence of thermonuclear ^{3}H in groundwater at depths of approximately 200 m (Mullican et al., in press). Rapid recharge in the Diablo Plateau relative to that in the Hueco Bolson is attributed to preferential flow along fractured limestones that are exposed in the arroyo floors, whereas clay beneath arroyo floors in the Hueco Bolson impedes recharge.

Chloride concentration in soil water beneath playas in eastern New Mexico was approximately 70 g m^{-3}, whereas that beneath nearby cover sands was approximately 1,000 g m^{-3} (Stone, 1990). These differences in chloride concentrations resulted in moisture fluxes that ranged from $\geq$12 mm yr^{-1} in the playas to 4 mm yr^{-1} in the sandy region. The moisture flux estimate for the playa is similar to estimates for the fissured sediments in the Hueco Bolson and is also a lower limit because chloride concentrations in runon were neglected. Sediments beneath the playas represent zones of enhanced moisture percolation as a result of prolonged periods of inundation.

Hydraulic data were used to compare moisture fluxes beneath a crater that was produced by nuclear explosions in the Nevada test site with moisture fluxes in undisturbed sediment profiles 200 m from the crater (Tyler et al., 1986). Soil texture was similar in both systems. Moisture content was as much as 15% higher under the crater than in the undisturbed sediments. Water potentials were approximately -0.1 MPa in sediments beneath the crater and -10 to -50 MPa in the undisturbed sediments. Estimates of moisture flux beneath the crater ranged from 0.5 to 4 m yr^{-1} and show enhanced downward water movement in these disturbed sediments.

The range of chloride concentrations in secondary sinkholes (20 to 100 g m^{-3}) in a semiarid region of South Australia differed markedly from that in surrounding geomorphic settings (0 to 200,000 g m^{-3}) (Allison et al., 1985). Moisture fluxes based on the chloride mass balance approach ranged from 0.1 mm yr^{-1} in undisturbed calcrete and vegetated dunes to $\geq$ 60 mm yr^{-1} in secondary sinkholes.

The estimate for the sinkholes is a minimum value because the effect of chloride in runon into the sinkhole was not included. Variations in calculated moisture fluxes between the secondary sinkholes in South Australia and the fissured sediments in the Hueco Bolson reflect differences in estimated Cl concentration in precipitation between the two areas (South Australia, 4.3g m^{-3}; Hueco Bolson 0.29g m^{-3}). The secondary sinkholes, like the fissured sediments and underlying fractures in the Hueco Bolson, act as preferred pathways for downward water movement.

Results from these studies have important implications for unsaturated flow and solute transport in semiarid and arid regions. The large range of moisture fluxes in each of the study areas discussed demonstrates the importance of preferential pathways in enhancing water percolation. On the scale of these study areas, water does not move as a piston but is concentrated in fissured sediments, playas, sinkholes, and craters. Because of their lower elevations, these geomorphic systems collect surface runoff, and they are inundated for longer time periods and under higher head than surrounding sediments. Disturbed soil in craters, or cavities in sinkholes, and loosely filled fractures beneath fissures, further contribute to higher percolation rates. The spatial variability in moisture flux in each of these study areas indicates that areal average moisture fluxes are meaningless in terms of recharge and contaminant transport. Higher moisture fluxes along preferred pathways reduce the effectiveness of thick unsaturated zones in attenuating contaminants, and characterization of these preferred pathways is critical in assessing the suitability of sites for waste disposal.

CONCLUSIONS

Fissured sediments in the Chihuahuan Desert act as preferred flow pathways, as indicated by comparison of hydraulic and chemical data in the fissured sediments with data from sediments underlying nearby arroyos, ephemeral streams, and interstreams. Water potentials were generally higher beneath the fissures than beneath ephemeral streams and interstreams. Lower maximum chloride concentrations in the fissured area (80 to 105 g m^{-3}) relative to other geomorphic settings (2,000 to 6,000 g m^{-3}) were attributed to leaching of chloride. Calculated moisture fluxes based on chloride data for the fissured sediments ranged from 1 to 8 mm yr^{-1} and were as much as 350 times higher than those calculated for ephemeral stream and interstream sediments. Moisture velocities in the fissured sediments ranged from 10 to 70 mm yr^{-1}. A tracer experiment in a fissure showed higher moisture and solute transport in the underlying fracture-fill sediments than in adjacent sediments. Two-dimensional simulations with the computer code

TRACR3D indicated that the effective hydraulic conductivity of the fracture fill was at least 10 times greater than that in adjacent sediments. Numerical simulations of the ponding experiment reproduced the general shape of the solute plume. The distribution of the solute was most sensitive to spatial variability in soil type and corresponding hydraulic parameters and was relatively insensitive to variations in the initial water potentials (-2 MPa $\leq \psi \leq -0.1$ MPa) and pond depth (0.01 to 0.8 m). The results of this study suggest that the fissured sediments act as preferred pathways for moisture and solute movement.

Comparisons with preferential flow pathways such as arroyos, craters, and sinkholes in other regions suggest that the primary controls on the percolation rates are the duration of inundation and the presence of subsurface structures such as fractures or sinkholes that allow rapid water and solute movement. The distribution of these zones of enhanced moisture flux is critical in assessing the suitability of a site for waste disposal because flow along these pathways short-circuits the system and would result in rapid transmission of contaminants through the unsaturated zone.

ACKNOWLEDGEMENTS

REFERENCES

Allison, G.B., Stone, W.J. and Hughes, M.W., 1985. Recharge in karst and dune elements of a semi-arid landscape as indicated by natural isotopes and chloride. J. Hydrol., 76: 1-26.

Baumgardner, R.W., Jr. and Scanlon, B.R., in press. Surface Fissures in the Hueco Bolson and Adjacent Basins, West Texas. Univ. Texas Austin, Bur. Econ. Geol.

Bentley, H.W., Phillips, F.M. and Davis, S.N., 1986. 36Cl in the terrestrial environment. In: P. Fritz and J. -C. Fontes (Editors), H of Environmental Isotope Geochemistry. Elsevier, New York. pp. 422 -475.

Biggar, J.W. and Nielsen, D.R., 1967. Miscible displacement and leaching phenomenon. Agron. Monog. 11: 254-274.

Campbell, G.S., 1985. Soil Physics with Basic: Transport Models for Soil-Plant Systems: Elsevier, New York, 150 pp.

Dagan, G. and Bresler, E., 1979. Solute transport in unsaturated heterogenous soil at field scale. I. Theory. Soil Sci. Soc. Am. J. 43: 461-467.

Davenport, D.C., Martin, P.E. and Hagan, R.M., 1982. Evapotranspiration from riparian vegetation: water relations and irrecoverable losses for saltcedar. J. Soil & Water Conserv., 37: 233-236.

Davis, L.A. and Neuman, S.P., 1983. Documentation and user's guide: UNSAT2-variably saturated flow model: U.S. Nucl. Reg. Comm. Rept. No. NUREG/CR-3390.

Folk, R.L., 1974. Petrology of Sedimentary Rocks: Hemphill, Austin, Texas, 182 pp.

Gay, L.W. and Fritschen, L.J., 1979. An energy budget analysis of water use by saltcedar. Water Resour. Res., 15: 1589-1592.

Gee, G.W. and Hillel, D., 1988. Groundwater recharge in arid regions: review and critique of estimation methods. Hydrol. Proc., 2: 255-266.

Germann, P.F., 1988. Approaches to rapid and far-reaching hydrologic processes in the vadose zone. J. Contam. Hydrol., 3: 115-127.

Glass, R.J., Steenhuis, T.S. and Parlange, J.Y., 1988. Wetting front instability as a rapid and far-reaching hydrologic process in the vadose zone. J. Contam. Hydrol., 3: 207-226.

Jachens, R.C. and Holzer, T.L., 1979. Geophysical investigations of ground failure related to ground-water withdrawal—Picacho Basin, Arizona. Ground Water, 17: 574-585.

Jury, W.A. and Roth, K., 1990, Transfer Functions and Solute Transport Through Soil: Theory and Applications. Birkhauser, Basel. 328 pp.

Larson, M.K. and Pewe, T.L., 1986. Origin of land subsidence and earth fissuring, northeast Phoenix, Arizona. Assoc. Engin. Geol. Bull., 23: 139-165.

Mattick, J.L., Duval, T.A. and Phillips, F.M., 1987. Quantification of groundwater recharge rates in New Mexico using bomb 36Cl, bomb 3H and chloride as soil-water tracers. Water Resour. Res. Inst. Rept. 220, Las Cruces, New Mexico, 184 pp.

Mualem, Y., 1976. A new model for predicting the hydraulic conductivity of unsaturated porous media. Water Resour. Res., 12: 513-521.

Mullican, W.F., III and Senger, R.K., in press. Hydrologic Investigations of Deep Ground-Water Flow in the Chihuahuan Desert, Texas. Univ. Texas Austin, Bur. Econ. Geol.

Mullican, W.F., III, Kreitler, C.W. and Nativ, R., in press. Hydrogeology of the Diablo Plateau, Texas. Univ. Texas Austin, Bur. Econ. Geol.

Narasimhan, T.N., Witherspoon, P.A. and Edwards, A.L., 1978. Numerical model for saturated-unsaturated flow in deformable porous media, 3. Applications. Water Resour. Res. 14: 1017-1034.

Nilsen, E.T., Sharifi, M.R. and Rundel, P.W., 1984. Comparative water relations of phreatophytes in the Sonoran Desert of California. Ecology, 65: 767-778.

Odening, W.R., Strain, B.R. and Oechel, W.C., 1974. The effect of decreasing water potential on net CO_2 exchange of intact desert shrubs. Ecology, 55: 1086-1095.

Philip, J.R., 1958. The theory of infiltration: 6. Effect of water depth over soil. Soil Sci., 85: 278-286.

Robinson, R.A. and Stokes, R.H., 1959. Electrolyte Solutions. Butterworths Publ., London, 571 pp.

Scanlon, B.R., in press. Evaluation of moisture flux from chloride data in desert soils. J. Hydrol.

Scanlon, B.R., Wang, F.P. and Richter, B.C., 1991. Field Studies and Numerical Modeling to Evaluate Controls on Unsaturated Flow: A Case Study, Chihuahuan Desert, Texas. Univ. Texas Austin, Bur. Econ. Geol., Rept. Inv. 199, 56 pp.

Schulin, R., Van Genuchten, M.Th., Fluhler, H. and Ferlin, P., 1987a. An experimental study of solute transport in a stony field soil. Water Resour. Res., 23: 1785-1794.

Schulin, R., Wierenga, P.J., Fluhler, H. and Leuenberger, J., 1987b. Solute transport through a stony soil. Soil Sci. Soc. Am. J., 51: 36-42.

Sharma, M.L. and Hughes, M.W., 1985. Groundwater recharge estimation using chloride, deuterium and oxygen-18 profiles in deep coastal sands of western Australia. J. Hydrol., 81: 93-109.

Stone, W.J., 1990. Natural recharge of the Ogalalla aquifer through playas and other non-stream-channel settings, eastern New Mexico. In: T. C. Gustavson (Editor), Geologic Framework and Regional Hydrology: Upper Cenozoic Blackwater Draw and Ogallala Formations, Great Plains, Univ. Texas Austin, Bur. Econ. Geol., pp. 180-192.

Travis, B.J. and Birdsell, K.H., 1991. TRACR3D 1.0: A Model of Flow and Transport in Porous Media, Model Description and User's Manual. Los Alamos Natl. Lab., Rept. No. LA-11798-M, 110 pp.

Tyler, S.W., McKay, W.A., Hess, J.W., Jacobson, R.L. and Taylor, K., 1986. Effects of surface collapse structures on infiltration and moisture redistribution. Water Resour. Center, Desert Research Inst., Univ. Nevada, Rept. No. 45058.

U.S. Army Corps of Engineers, Hydrologic Engineering Center. 1981. HEC-1 Flood hydrograph package: Davis, CA, 190 pp.

⸺, 1982. HEC-2 Water surface profiles: Davis, CA,, 40 pp.

U.S. Department of Agriculture, 1975. Soil Taxonomy. Soil Conservation Service, Washington, D.C., 754 pp.

Van Genuchten, M.Th., 1980. A closed-form equation for predicting the hydraulic conductivity of unsaturated soils: Soil Sci. Soc. Am. J., 44: 892-898.

Van Genuchten, M.Th., 1985. RETC.F77: A Program to Analyze Observed Soil Water Tension and Hydraulic Conductivity Data. U.S. Salin. Lab., Riverside, Calif. Spec. Rept.

Wierenga, P.J. and Van Genuchten, M.Th., 1989. Solute transport through small and large unsaturated soil columns. Ground Water, 27: 35-42.

Yeh, G.T. and Ward, D.S., 1979. FEMWATER: A Finite Element Model of Water Flow through Saturated-Unsaturated Porous Media: Oak Ridge Natl. Lab. Rept. No. ORNL-5567.